Вараксин С. Проникновение улучшения грунта в область глубоких фундаментов // Construction and Geotechnics. – 2020. – Т. 11, № 4. – С. 106–125. DOI: 10.15593/2224-9826/2020.4.09

Varaksin S. The penetration of ground improvement into the realms of deep foundations. *Construction and Geotechnics*. 2020. Vol. 11. No. 4. Pp. 106-125. DOI: 10.15593/2224-9826/2020.4.09

CONSTRUCTION AND GEOTECHNICS
Т. 11, № 4, 2020
http://vestnik.pstu.ru/arhit/about/inf/

DOI: 10.15593/2224-9826/2020.4.09
УДК 624.138, 624.154

ПРОНИКНОВЕНИЕ УЛУЧШЕНИЯ ГРУНТА В ОБЛАСТЬ ГЛУБОКИХ ФУНДАМЕНТОВ

Серж Вараксин

Научные комитеты TC211, TC102, Франция

О СТАТЬЕ

Получена: 08 августа 2020
Принята: 29 ноября 2020
Опубликована: 30 декабря 2020

Ключевые слова:

улучшение грунта, цементный столб, жесткие включения, свая, фундамент.

АННОТАЦИЯ

Инженерами в течение многих десятилетий систематически используется улучшение грунта как средство, позволяющее заменить свайный фундамент на фундамент мелкого заложения. Некоторые методы улучшения грунта, которые производятся с помощью буровых установок и представляют собой столбчатые твердые включения в виде цементных столбов, затрудняют различие того, где заканчивается улучшение грунта и начинается глубокий свайный фундамент. Эта статья поможет сориентироваться инженеру-геотехнику, рассматривая концепции жестких включений, их отличия от свай и представляя тематические исследования применений очень глубоких жестких включений.

THE PENETRATION OF GROUND IMPROVEMENT INTO THE REALMS OF DEEP FOUNDATIONS

Serge Varaksin

TC211, TC102, France

ARTICLE INFO

Received: 08 August 2020
Accepted: 29 November 2020
Published: 30 December 2020

Keywords:

ground improvement, cementituous columnar, rigid inclusions, pile, foundation.

ABSTRACT

Ground improvement as a means for allowing the replacement of piled foundations with shallow footings is systematically being used by engineers for many decades. Some ground improvement techniques that are installed by piling rigs and include cementituous columnar rigid inclusions makes it difficult to distinguish where ground improvement ends and deep piled foundations commence. This paper assists the geotechnical engineer by reviewing the concepts of rigid inclusions, how they differ with piles, and presenting of case studies of very deep applications of rigid inclusions.

© **Вараксин Серж** – научный советник комитетов TC211, TC102, e-mail: s.varaksin@apageo.com.

Serge Varaksin – Scientific Advisor Coremember TC211, TC102, e-mail: s.varaksin@apageo.com.

1. Introduction

The best ground conditions for a project can be envisaged to be when the ground is competent and loads can be applied to shallow footings. In this scenario construction time and costs are both minimal. Terzaghi et al. [1] define a shallow footing as a footing that has a width equal to or greater than the foundation depth, which is the distance from the level of the ground surface to the base of the footing, and a pile as a very slender pier that transfers a load through its lower end onto a firm stratum or else through side friction onto the surrounding soil. Bowles [2] defines shallow foundations as bases, footings, spread footings or mats with the ratio of depth of footing to its width being equal to or less than 1, and deep foundations as piles, drilled piers or caisson with ratio of length to width (or diameter) being equal to or greater than 4. On the other hand, Das [3] states that studies show that the ratio of footing depth to width of shallow footings can be as large as 3 or 4.

While it could be advantageous to have concise definitions for various concepts and behaviours to avoid confusion and to allow clear communication, it is not possible to simply set an integer as the boundary between two foundation systems. The concept of shallow versus deep foundation is only a simplification for explaining the mechanisms of load transfer to the ground. Bearing of shallow foundations are generally expressed by shear theories originally developed by Prandtl [4], Terzaghi [5], Meyerhof [6] and Hansen [7]. Skin resistance (Tomlinson [8], Vijayvergiya and Focht [9], Burland [10]) may become a major contributor as the ratio of footing height to width begins to increase. At the same time, while a large based footing may be categorised as a shallow foundation system due to its depth to width ratio, the depth of soil within the system may be very deep indeed.

To further complicate this simplification, it is possible to convert deep loose or soft soils to adequately competent ground by soil improvement, and to safely dissipate the loads without engaging piles for transferring loads to firm ground. Chu et al. [11] have classified and described the various ground improvement techniques that are commonly practiced. Some of these techniques are developed to improve the physical and mechanical properties of in-situ soils without the introduction of imported material, and the outcome will remain as what is classically referred to as a shallow foundation. On the other hand, in other ground improvement techniques higher quality materials are added to the ground as inclusions. Some inclusions may be very long, and can form deep foundations that are composed of classical shallow footings and deep soil masses that are improved by the inclusions. These types of foundations cannot be expressed by the classical shallow foundation approaches and require further understanding, analysis and design of the improved ground as part of the foundation system.

The complication in the categorisation can turn into confusion when piling rigs are used to install cementitious columnar inclusions. One very efficient, beneficial and affordable type of such rigid inclusions is the *controlled modulus column* (*CMC*).

2. Controlled Modulus columns

2.1. Construction of CMC-Type Rigid Inclusions

As shown in Figure 1, a controlled modulus column is installed in soft ground using a specially designed auger that is composed of a helical tip and a cylindrical hollow stem follow-up section. As the auger is thrust and screwed into the soil, the cylindrical extension displaces the soil laterally and reduces the amount of spoil that is generated to negligible amounts compared to

cast in-situ piling solutions such as continuous flight auger (CFA) or bored piles. During the auger extraction, grout is pumped through the hollow stem and auger to form a columnar inclusion with a diameter that is usually 250 to 450 mm.

Fig. 1. CMC auger

The CMC rig should be able to provide a continuous down pull with a high torque in rotation. Further enhancements to the equipment can include a radio control unit to allow the rig operator to directly command the concrete pump from his control panel. The control panel displays torque, speed, depth, down pull force, grout pressure and volume of pumped grout.

2.2. Advantages of Controlled Modulus Columns

Stone column stability is reliant on the horizontal containment of the soil (Barksdale and Bachus [12]), deep soil mixing column strength is dependent on the in-situ soil properties (Navin [13]); however, similar to piles, CMCs do not rely on soil parameters for lateral stability nor are their strengths affected by the surrounding soil.

As any concrete product, CMC modulus of deformation is a function of the concrete strength (American Concrete Institute [14]). Masse et al. [15] state that the deformation moduli of CMCs are typically 50 to 3,000 times that of the weakest soil stratum; hence, this type of inclusion reduces settlements more efficiently than other techniques in which inclusions are of stone or a mixture of added material and in-situ soil. Alternatively, with a different perspective, it is possible to reduce ground settlements using a lower replacement ratio (Murayama [16]; Aboshi et al. [17]).

Reaching the required size, mix or strength of ground improvement techniques with additives or inclusions is usually timely compared to CMCs. For example, introducing and compacting stone for the construction of stone columns must be carried out in numerous lifts, and sufficient time must be allocated to enlarge the column size and appropriately compact the stones in each lift. Similarly, grout that is produced for jet grouting or deep soil mixing must be progressively mixed with in-situ soil, which results in lesser quantities of placed inclusions per unit time. However, concrete for installing CMCs is produced in a factory (batching plant), and placing material is performed with the same speed as CFA piling.

The amount of vibration that is generated by CMC installation is comparable with CFA piling as the installation process itself is vibration free and the rig is essentially the same for both techniques.

The main advantages of CMCs can thus be summarised as:

2.3. Pile versus CMC

Whilst CMC's and piles may look very similar in appearance, there design concepts are very different. As shown in Figure 2 (*a*), in piled foundations, it is typically assumed that loads are almost entirely transferred to competent ground layers through the piles and pile caps. However, it can be seen in Figure 2 (*b*) that in foundations with inclusions the loads are distributed by arching (Hamidi et al. [18]) between the in-situ soft soil and inclusions through a well compacted granular transition layer, which is also called the load transfer platform (LTP).

Whilst the concept, behaviour, design, requirements and functionality of CMCs are not the same as piling, with consideration that the scope of most standards do not cover CMCs, the authors have come across many cases where engineers erroneously attempt to extend piling code requirements to CMCs. This will usually result in poor engineering that defies the advantages of ground improvement and reverts the concept and design back into piles.

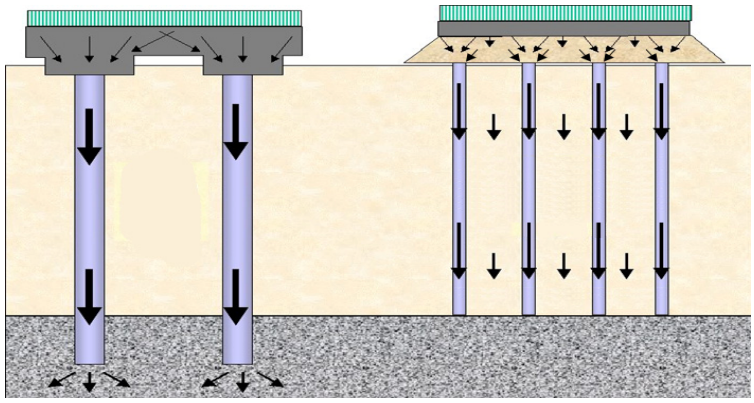

a *b*

Fig. 2. Load transfer in (*a*) piled foundations and (*b*) ground improved by rigid inclusions

2.4. CMC Concept

Combarieu [19] studied the behaviour of rigid inclusions in soft ground. Figure 3 shows that a compressible ground with thickness H that is subjected to an embankment load with intensity q_o will ultimately undergo a settlement on the surface that can be denoted by W_s (o). Similarly, settlement at any depth, z, can be denoted by W_s (z). The soil conditions at distances away from the single inclusion are identical to untreated ground after complete stabilisation. However, the stress and deformations change around the immediate vicinity of the inclusion. The inclusion settles by an amount equal to W_p (z) due to the load it has been subjected to and by a small amount due to its own compression. The settlement is higher when the rigid inclusion terminates in soft soil (Figure 4) compared to when it is rests on hard soil (Figure 5).

If h_c is the depth where the inclusion and soil settle equally, at the lower part of the inclusion where $z > h_c$, the settlement of the soil is less than the inclusion settlement and its compression; however, the opposite is true in the upper portion where $z < h_c$.

Ultimately, as shown in Figure 6, the four forces acting on the inclusion at equilibrium are:

- Driving forces: The vertical load Q acts on the head of the inclusion and the resultant negative friction, F_n, acts along the inclusion segment with length h_c.
- Resisting forces: Positive friction, F_p, is mobilised in the lower part of the inclusion and along a segment with length $L - h_c$, and Q_p acts at the base of the inclusion. The balance of the forces is $Q + F_n = F_p + Q_p$.

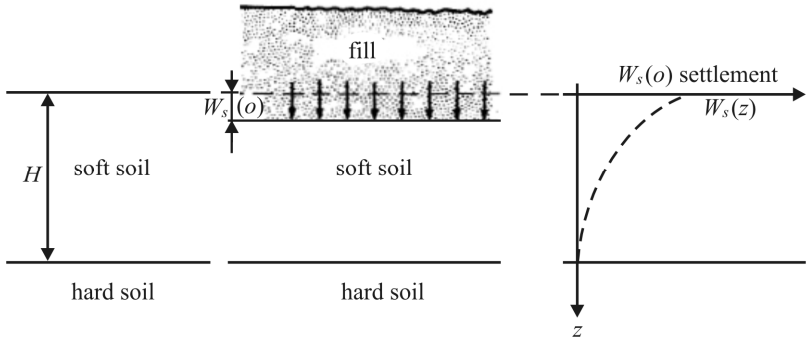

Fig. 3. Ground section without rigid inclusion (Combarieu, 1988)

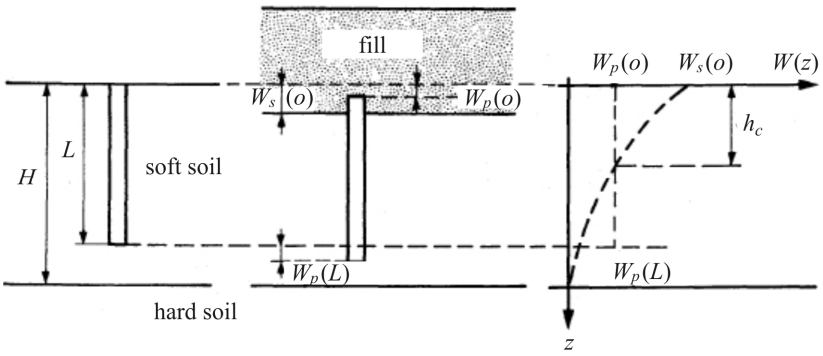

Fig. 4. Ground section with rigid inclusion terminating in soft ground (Combarieu [19])

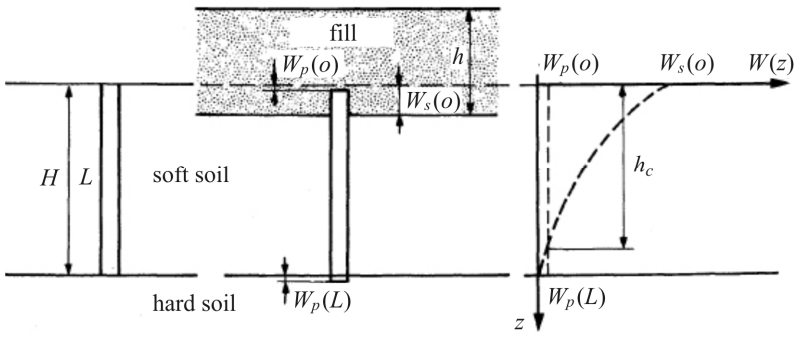

Fig. 5. Ground section with rigid inclusion supported by hard ground (Combarieu [19])

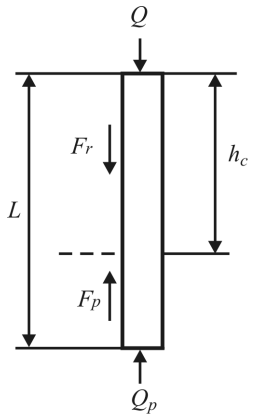

Fig. 6. Forces acting on a rigid inclusion (Combarieu [19])

The behaviour of rigid inclusions, inclusive of CMCs, without rigid connections to the structure has been the subject of an extensive French national research programme called ASIRI (*Améliorations de Sols par Inclusions RIgides*, which translates to *Soil Improvement by Rigid Inclusions*) (IREX [20]).

2.4.1. Behaviour of the Load Transfer Platform and Failure Mechanisms

As shown in Figure 7, it is assumed that CMCs with diameter $D = 2r_p$ are installed in a square grid with centre to centre spacing s. LTP thickness is denoted by H_M, and is defined by its characteristics (cohesion c', friction angle φ' and volumetric weight γ). The uniformly distributed external load q_o is applied to the LTP.

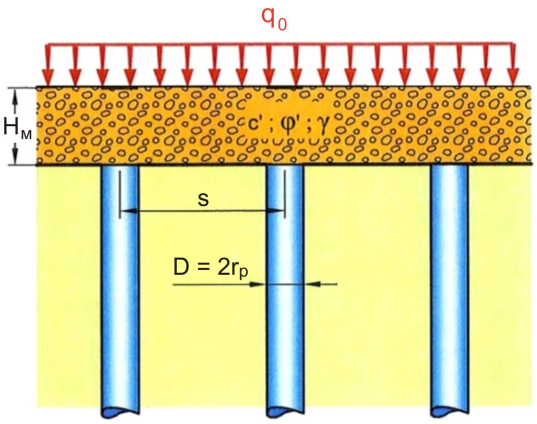

Fig. 7. Section showing ground improved by rigid inclusions,
LTP and uniform loading (IREX [20])

ASIRI has shown that whilst the actual equilibrium diagram is dependent on the geometry and nature of the loading, as shown in Figure 8, failure can be by two mechanisms; i.e. Prandtl's failure mechanism [4] or punching shear.

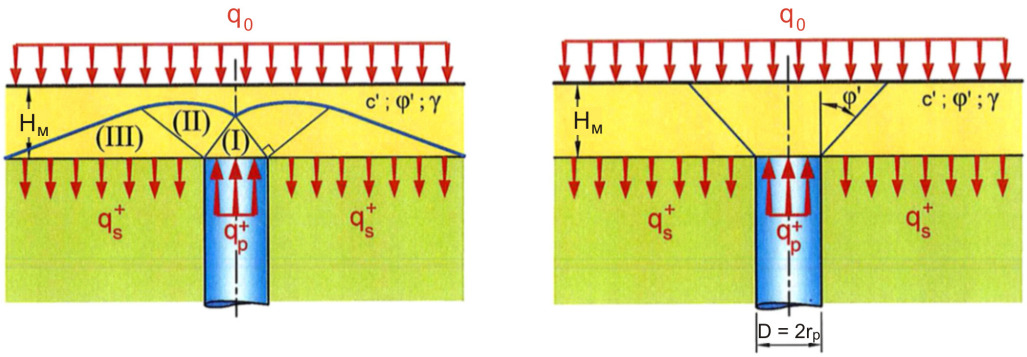

a *b*

Fig. 8. (*a*) Prandtl failure mechanism for slabs on grade, rafts, footings and thick embankments and (*b*) punching shear failure mechanism for thin embankments (IREX [20])

2.4.1.1. Prandtl's Failure Mechanism

Prandtl's failure mechanism [4] occurs when the LTP is covered by a rigid structural element such as a slab on grade, raft or footings, or when the embankment is sufficiently thick to avoid punching failure, which corresponds to the formation of shear cones in the LTP's surface. ASIRI implies that an embankment is considered thin when:

$$H_M < 0,7(s - D) \tag{1}$$

Figure 8 (*a*) shows that Prandtl's failure diagram includes a Rankine active limit state domain (I) above the inclusion head that is delimited by a logarithmic spiral arc domain (II) and a Rankine passive limit state domain (III), which is located beyond the inclusion head. q_p^+ is the stress at the inclusion head and q_s^+ is the stress on the in-situ soil.

ASIRI has been developed in line with Eurocode. The maximum load that can be applied to the inclusion head q_p^+ is therefore calculated in ULS (Ultimate Limit State) condition. This verification is performed by implementing Eurocode 7 Design Approach 2 (European Standard [21]) with the combination of partial factors being *A1* + *M1* + *R2* (*A* for Action, *M* for Material and *R* for Resistance). This means that load factors on dead and live loads are respectively 1.35 and 1.50 and that no partial factor is applied to the materials. According the Prandtl's diagram, q_p^+ can be determined from the stress applied on the supporting soil and the intrinsic parameters of the LTP:

$$q_p^+ = s_q N_q q_s^+ + s_c N_c \frac{c'}{\gamma_{c'}} - s_\gamma N_\gamma r_p \frac{\gamma}{\gamma_\gamma} \tag{2}$$

N_q, N_c and N_γ are coefficients that are functions of the friction angle of the LTP, and can be calculated from Equations 3 to 5:

$$N_q = \tan^2\left(\frac{\pi}{4} + \frac{\varphi' / \gamma_{\varphi'}}{2}\right) \times e^{\pi \tan\left(\varphi' / \gamma_{\varphi'}\right)} \tag{3}$$

$$N_c = (N_q - 1)\cot\left(\varphi' / \gamma_{\varphi'}\right) \tag{4}$$

$$N_\gamma = 2(N_q - 1)\tan\left(\varphi' / \gamma_{\varphi'}\right) \tag{5}$$

$\gamma_{c'}$, $\gamma_{\varphi'}$, and γ_γ are material partial factors and equal to 1.

The LTP's weight is typically neglected for a relatively thin platform, and the superficial (third) term in Equation 2 is omitted.

For purely granular LTP, there is no cohesion, and the related term becomes null. Hence, Equation 2 becomes:

$$q_p^+ = s_q N_q q_s^+ \tag{6}$$

For axisymmetric or plane-strain conditions, $s_q = 1$, and a relationship that is only a function of φ' is established in the form of Equation 7 between q_p and q_s.

$$q_p^+ = N_q q_s^+ \tag{7}$$

Solving the problem and determining the values of q_p and q_s requires a second equation. Using load conservation:

$$\alpha q_p^{+} + (1-\alpha) q_s^{+} = q_o \tag{8}$$

α = replacement ratio

$$\alpha = \frac{A_c}{A_c + A_s} \tag{9}$$

A_c = area of inclusion
A_s = area of soil
From Equations 7 and 8:

$$q_p^{+} = \frac{N_q}{1+\alpha(N_q - 1)} q_o^{+} \tag{10}$$

$$q_s^{+} = \frac{1}{1+\alpha(N_q - 1)} q_o^{+} \tag{11}$$

Research on Prandtl's failure mechanism has been further carried out by centrifugal testing with various LTP thicknesses, rigid inclusion spacing and replacement ratios within the ASIRI programme (Okyay [22]). Centrifuge test results are compared with limiting pressures calculated from Prandtl's theory in Figure 9. It can be seen that a very good agreement exists between measured and theoretical values.

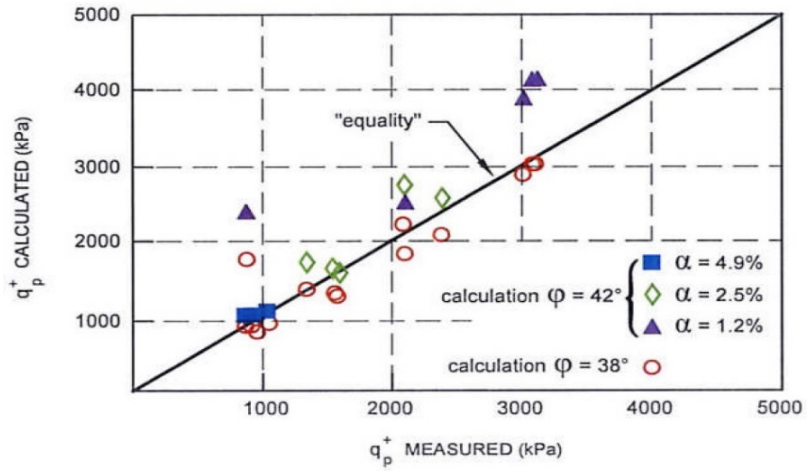

Fig. 9. Comparison of measured limiting pressures with theoretical values calculated from Prandtl's theory (IREX [20])

Prandtl's approach was also investigated by performing finite element calculations for various uniformly distributed loads. Figure 10 shows the pressures acting on the soil and on the inclusion head respectively on the abscissa and ordinate. The blue curve shows Equation 7, the slanted black lines correspond to Equation 8, and the pink line is derived from finite element calculations. This figure also shows the stresses on the soil and inclusion and the value that can be mobilised at the head of the inclusion.

During the investigation, the Young modulus of the compressive soil was reduced for each uniform loading until the LTP failed. It was observed that at the last step prior to failure the stress

at the inclusion head approached Prandtl's limit, but did not intersect it. Prandtl's failure mechanism can also be visualised by the distribution of the plastic points that are shown as red dots in Figure 10.

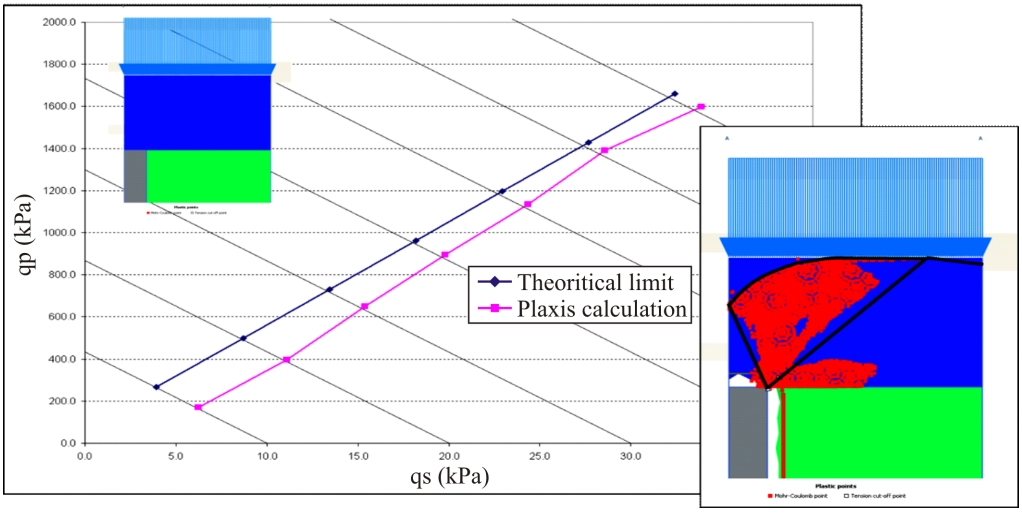

Fig. 10. Comparison of limiting pressures calculated from finite element analyses and Prandtl's theory (IREX [20])

2.4.1.2. Punching Shear Failure Mechanism

Figure 8 (b) shows that the second failure mechanism can be modelled by a vertical cone within the LTP layer. This mechanism exists only for thin LTPs that are not covered by rigid structural elements, and is associated with the peak friction angle of the material.

According to Eurocode 7 Design Approach 2 and from the shear cone geometry, the limit stress at the inclusion head is determined using the applied external load, q_o, the LTP's thickness, and the platform parameters.

In Figure 11:

$$R_c = R_p + H_M \tan\left(\frac{\varphi'}{\gamma_{\varphi'}}\right) \tag{12}$$

$$R = \frac{s}{\sqrt{\pi}} \tag{13}$$

$\gamma_{c'}$, $\gamma_{\varphi'}$, and γ_γ are material partial factors and equal to 1.

If, as shown in Figure 11 (*a*), the shear cones do not overlap if $H_M < H_c$, where:

$$H_c = \frac{R - r_p}{\tan\varphi'} \tag{14}$$

Then q_p^+ = weight of the cone plus the external load applied on the top circular side of the cone. Thus:

$$q_p^+ = \frac{H_M}{3}\left(\frac{R_c^2}{r_p^2} + 1 + \frac{R_c}{r_p}\right)\frac{\gamma}{\gamma_\gamma} + \frac{R_c^2}{r_p^2}q + \frac{1}{\tan\varphi'}\left(\frac{R_c^2}{r_p^2} - 1\right)\frac{c'}{\gamma_{c'}} \tag{15}$$

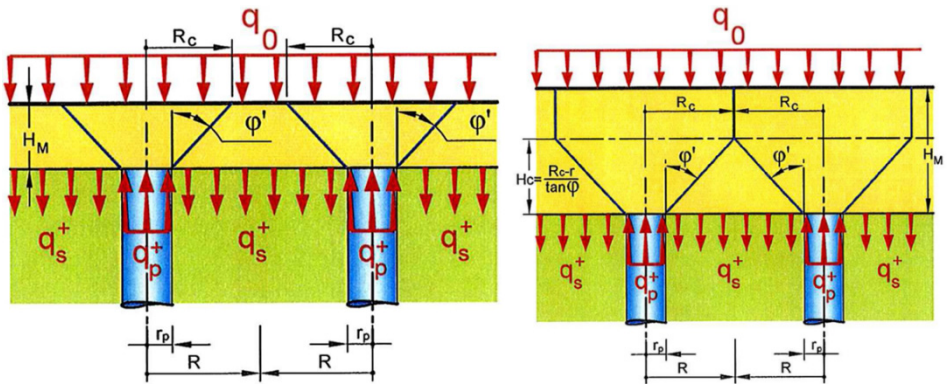

a *b*

Fig. 11. (*a*) Non-overlapping failure cones and (*b*) Overlapping failure cones (IREX [20])

As shown in Figure 11 (*b*), the shear cones overlap if $H_M > H_c$, where:

$$H_c = \frac{R_c - r_p}{\tan\varphi'} \tag{16}$$

$R_c = R$

q_p^+ = weight of the cone, weight of the soil cylinder above it and the external load multiplied by the unit cell area; therefore:

$$q_p^+ = \left[\frac{H_M}{3}\left(\frac{R^2}{r_p^2}+1+\frac{R}{r_p}\right)+(H_M - H_c)\frac{R^2}{r_p^2}\right]\frac{\gamma}{\gamma_\gamma}+\frac{R^2}{r_p^2}q_o+\left[\frac{1}{\tan\varphi'}\left(\frac{R^2}{r_p^2}-1\right)\right]\frac{c'}{\gamma_{c'}} \tag{17}$$

2.4.2. Ultimate Limit State (ULS) Stress Domain

When failure is by Prandtl's mechanism, regardless of the load level, the stress domain in the LTP is firstly limited by the Prandtl line, which was presented in Equation 7. The stress on the in-situ soil, q_s^+, is limited at ULS by the allowable stress $\sigma_{v;d}$, which can be determined with the appropriate partial factors from P_{LM}, the limit pressure of Menard pressuremeter test. q_p^+ is also limited by the load-bearing capacity of the inclusion and the allowable stress in the inclusion material. The first limitation is the load bearing capacity as per Eurocode 7. The second limitation, f_{cd}, is the allowable stress in the material as per Eurocode 2 (European Standard [23]). The stress domain is graphically shown in Figure 12.

$$q_{p\max} = \min\left[\frac{R_b/\gamma_b\cdot\gamma_{R,d} + R_s/\gamma_s\cdot\gamma_{R,d}}{\pi R_c^2}; f_{cd}\right] = \min\left[\frac{R_b/1.375 + R_s/1.375}{\pi R_c^2}; f_{cd}\right] \tag{18}$$

$$\sigma_{v;d} = \frac{k_p P_{LM}}{\gamma_{R;v}\cdot\gamma_{R,d}} = \frac{k_p P_{LM}}{1,4\times 1,2} = \frac{k_p P_{LM}}{1,68} \tag{19}$$

When the LTP is not covered by a rigid structural element, this domain may be partially limited. For example, as shown in Figure 13, if the LTP is thin, there are not any rigid structural elements, and failure cones do not overlap, then the stress domain is further limited by

the dashed blue line that corresponds to Equation 15. As a second example that is shown as dashed red lines in Figure 14, further limitations of Equation 17 are applied when the failure cones overlap.

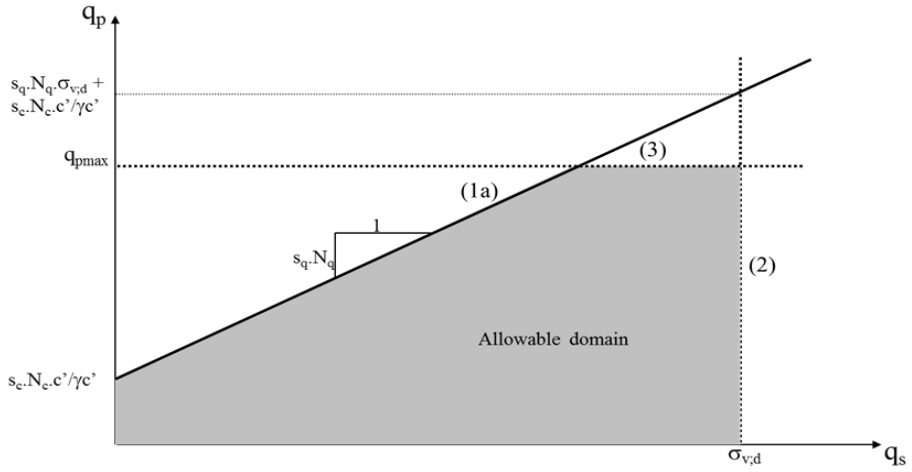

Fig. 12. ULS stress domain (IREX [20])

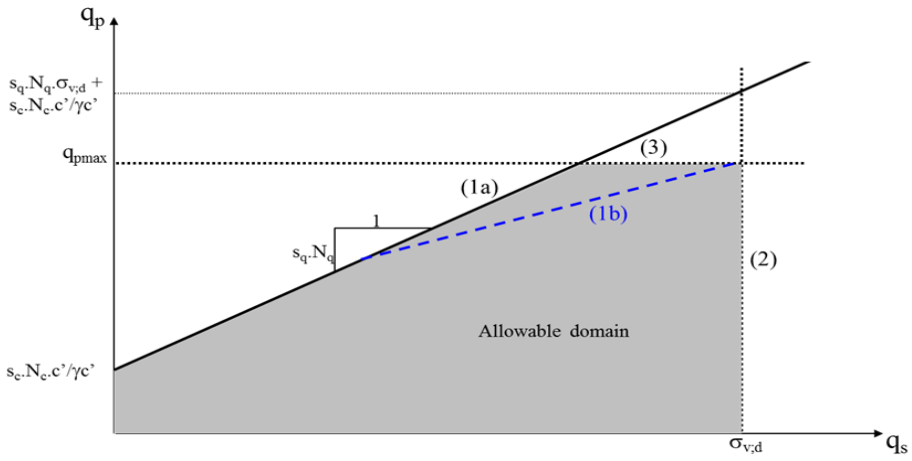

Fig. 13. ULS stress domain when LTP is thin, without rigid structural elements and with non-overlapping failure cones (IREX [20])

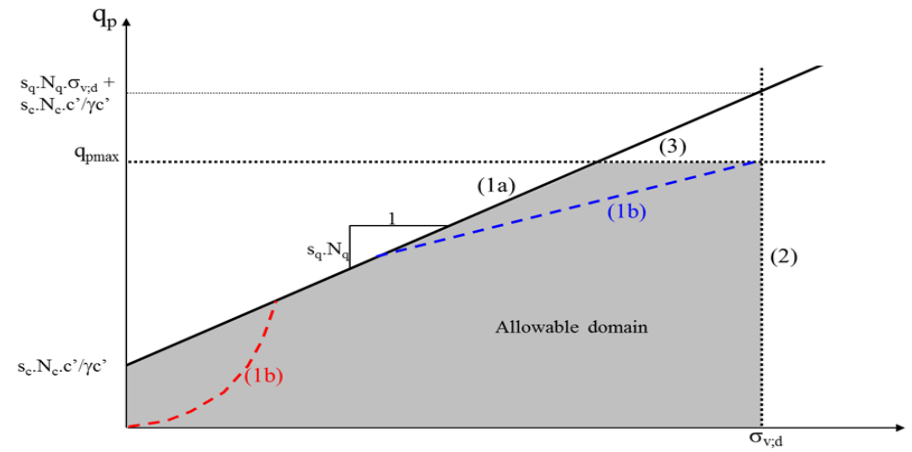

Fig. 14. ULS stress domain when LTP is thin, without a rigid structural element, and failure cones overlap (IREX [20])

To satisfy the load conservation equation, q_s^+ and q_p^+ must be on the diagonal blue lines that are shown in Figure 15. Therefore, for a given load q, the permissible domain will reduce to these segments. The calculated design limit $q_{p,d}^+$ is calculated by solving simultaneous equations of Prandtl and load conservation.

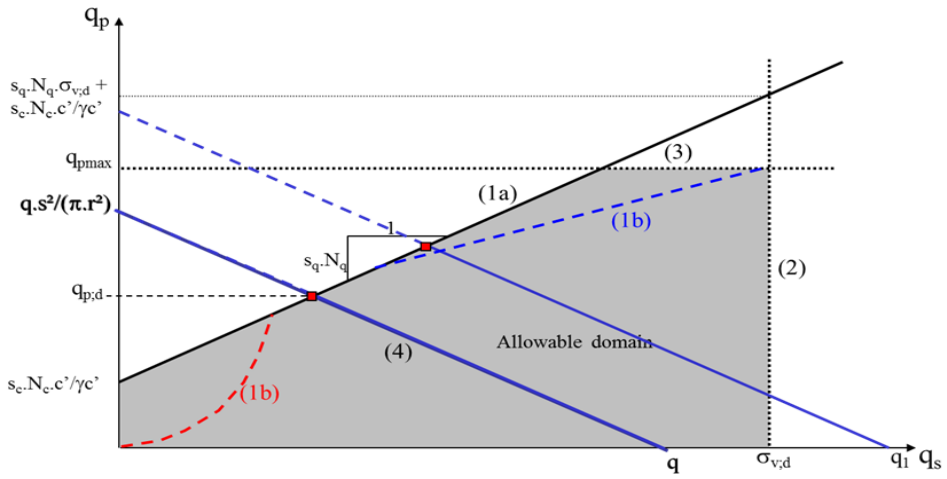

Fig. 15. ULS stress domain with consideration of the load conservation equation when LTP is thin, without a rigid structural element, and failure cones overlap (IREX [20])

$q_{p,d}^+$ is a function on q, the system geometry (CMC grid size and thickness of LTP) and the LTP parameters, but is independent of the deformability of the various soil layers. Whilst the intersection of Prandl's line (Equation 15) and the load conservation line (Equation 8) is $q_{p,d}^+$, the stress pair (q_p^+, q_s^+) that is actually mobilised can be anywhere on this diagonal segment, and its actual position will depend on the compressibility of the various soil layers directly below the LTP. In soft soil the mobilised pair will be close to $q_{p,d}^+$, and in dense soil it will be away from the limit.

It is important to understand that, as shown in Figure 16, changes of the external load move the equilibrium in the plane (q_p^+, q_s^+) along a curve that tends towards an asymptote for large loads; i.e. an increase in loading also increases the efficiency towards its maximum value, but is never able to create an internal failure of the LTP by intersecting with Prandtl's line.

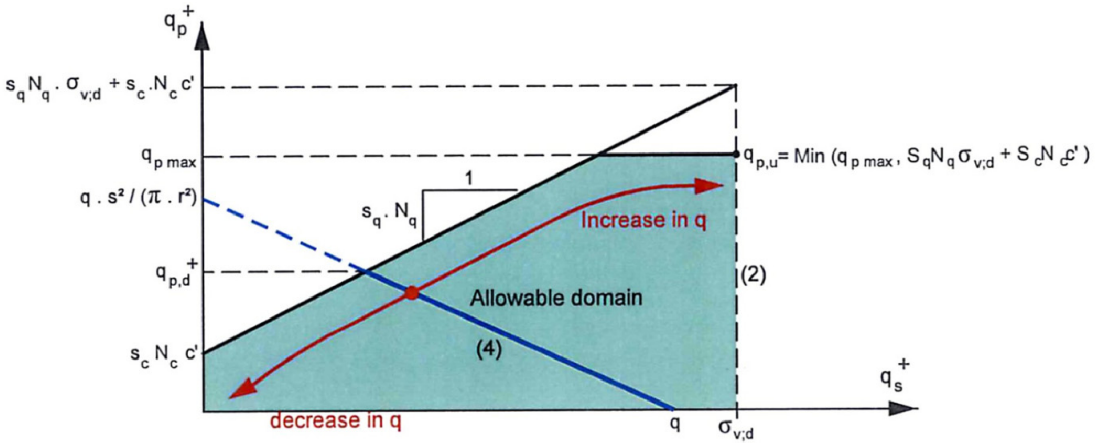

Fig. 16. $q_{p,d}^+$ and deformability of various soil layers (IREX [20])

2.4.3. Edge Behaviour

Stress distribution at the edge of the loading zone, where Prandtl's failure mechanism does not fully develop is somewhat different. The horizontal length of the Prandtl curve, L_{max}, is formulated in Equation 20. Figure 17 (*a*) shows that Prandtl's mechanism can fully develop in the LTP, and the limit pressure at the CMC head will be as discussed in the earlier sections if the overhang length of the footing, L, is greater than $L_{\max}$. In the extreme case that is shown in Figure 17 (*b*), the edge of the CMC corresponds to the edge of the footing; i.e. the overhang is zero, and the load applied to the footing is nearly fully transmitted on the CMC head. The vertical stress on the peripheral soil, which is due to the surrounding ground is equal to γH. IREX details the calculation process of N_q* with consideration of a LTP that is limited to the footing footprint. N_q* is assessed based on the friction angle at critical state of both the LTP (with φ_1) and the surrounding soil (with φ_2). N_q* values that are based on LTP and surrounding soil friction angles are shown in Table.

$$L_{\max} = \frac{\cos\left(\pi/4 - \varphi'/2\right)}{\cos\left(\pi/4 + \varphi'/2\right)} De^{-\tan(\varphi')\cdot\pi/2} \tag{20}$$

N_q* values based on LTP and surrounding soil friction angles

LTP φ_1	N_q* (φ_1)	Soil $\varphi_2 = 15^o$	Soil $\varphi_2 = 20^o$	Soil $\varphi_2 = 25^o$	Soil $\varphi_2 = 30^o$
		N_q*	N_q*	N_q*	N_q*
30	18.4	6.98	9.45	13.08	18.43
33	26.1	7.86	10.64	14.71	20.88
35	33.3	8.52	11.53	16.01	22.67
38	48.9	9.68	13.05	18.11	25.80
40	64.2	10.54	14.29	19.71	28.04

Figure 17 (c) shows that when the footing overhang is between 0 and $L_{\max}$, the limiting pressure at the CMC head can be estimated using a linear interpolation between these two extreme values. This is shown in Figure 18.

Generally, when more than one CMC is installed beneath the footing, the edge effect that has been described is applicable to only a fraction of the CMC depending on whether the CMC is at the footing corner or side (see Figure 19). The edge limit stress, q_p^+ (L), is applicable only to the exterior portion of the perimeter, the limit stress calculated from Prandtl's failure mechanism, q_p^+ (P), applies to the inner portion of the inclusion, and the resulting value must be a weighted average of these two terms.

By analogy with the distribution of negative friction within a group of piles, IREX proposes that limit stress values on the inclusion heads under the footing be determined using the weighting relationships shown in Equations 21 to 25.

For single row inclusions that are shown in Figure 20 (*a*):

$$q_{p,a}^+ = \frac{1}{3} q_p^+(P) + \frac{2}{3} q_p^+(L) \tag{21}$$

$$q_{p,e}^+ = \frac{2}{3} q_p^+(P) + \frac{1}{3} q_p^+(L) \tag{22}$$

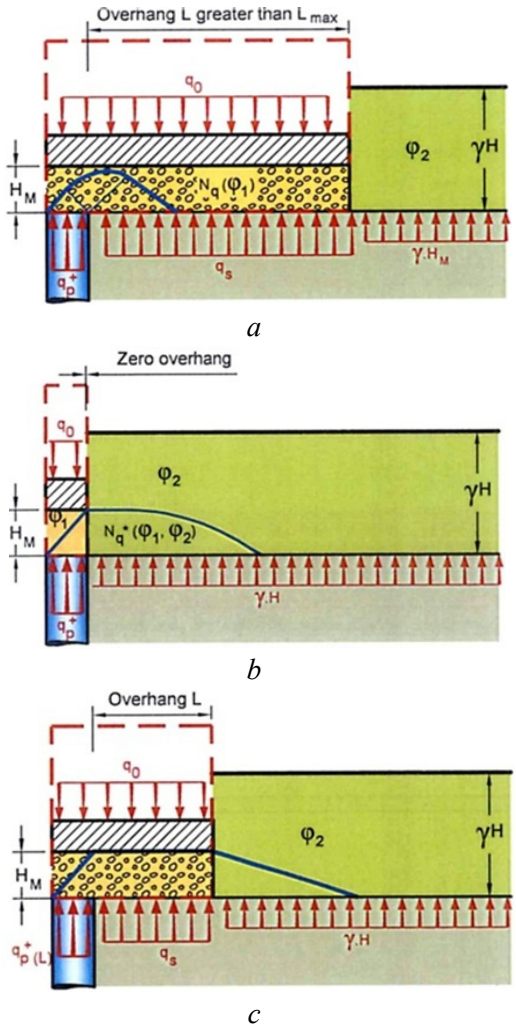

Fig. 17. Ground section at edge of rigid structural element (IREX [20])

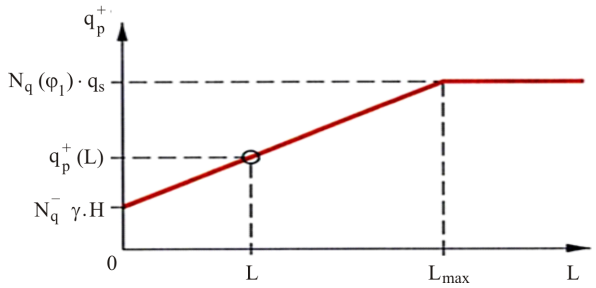

Fig. 18. Ground section at edge of rigid structural element (IREX [20])

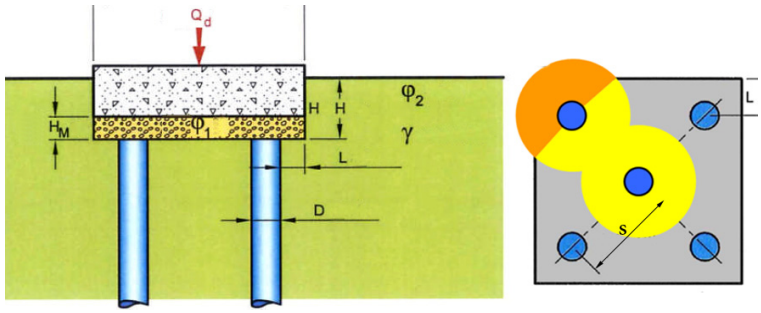

Fig. 19. Edge effect combination, modified from ASIRI (IREX [20])

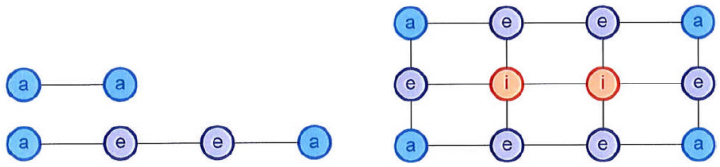

a *b*

Fig. 20. (*a*) Edge effect combination for single row of CMCs, (*b*) Edge effect combination for multiple rows of CMCs (IREX [20])

For multiple rows of inclusions that are shown in Figure 20 (b):

$$q_{p,i}^{+} = q_p^{+}(P) \tag{23}$$

$$q_{p,a}^{+} = \frac{7}{12} q_p^{+}(P) + \frac{5}{12} q_p^{+}(L) \tag{24}$$

$$q_{p,e}^{+} = \frac{5}{6} q_p^{+}(P) + \frac{1}{6} q_p^{+}(L). \tag{25}$$

2.5. Numerical Modelling

Whilst numerical methods are possibly the most popular analysis techniques that are currently practiced, their results are only as good as the model and the input parameters. Blind implementation of these calculation tools without in-depth understanding of the modelling process and suitability of the characteristic parameters may lead to unforeseen disastrous consequences.

Schweiger [24] has carried out a study on the outcomes of geotechnical problems that were numerically solved by a group of German engineers in his research programme. The first problem was the undrained analysis of a shield tunnel excavation for three conditions of elastic behaviour with no lining, elastic-perfectly plastic behaviour with no lining, and elastic-perfectly plastic behaviour with segmental lining. The problem was deliberately chosen to be very simple with constant undrained shear strength. Material parameters were also provided for all analyses. Review of results showed that in the elastic case there was a 20 % difference in maximum settlement of the ground surface above the tunnel, which was entirely due to the different lateral boundary condition assumptions. In the plastic solution the differences were significantly larger than the elastic case (76 to 159 mm), and the choice of the failure criterion being Von-Mises or Tresca had a notable impact. The results of this study suggested that, even for simple problems, the choice of the failure criterion is essential in non-linear analyses. The scatter in results was even larger in the third case, and surface settlement above the tunnel axis and at the crown ranged respectively from 1 to 25 mm and from 17 to 45 mm. In a second study Schweiger [24] studied the results of the analyses of a deep excavation problem in which the specifications, properties, stiffness, strength parameters and computational stages were given. Some of the engineers made extremely unrealistic assumptions for the material parameters, and were excluded. Scatter of results was also observed in this research, and review of the outcomes suggested that not only did the assumption of the constitutive model and the parameters have a significant influence on the results, but so did the manner in which the groundwater lowering was simulated.

Based on the review of a number of bored and driven piles and Menard pressuremeter test data (PMT) Frank and Zhao [25] have developed a method in which shaft friction mobilisation

curves and end load – end displacement curves are used to predict the load settlement curve of single piles under axial loading. These tri-linear curves are shown in Figure 21.

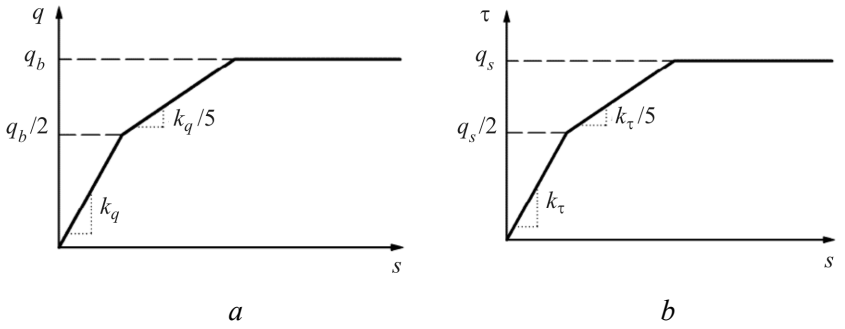

Fig. 21. (*a*) Pile toe stress versus settlement, (*b*) skin friction versus relative pile-soil displacement (Frank and Zhao [25])

The stiffnesses of the curves are:

- For fine grained soils: $k_\tau = 2E_M/B$ $k_q = 11E_M/B$
- For granular soils: $k_\tau = 0.8\ E_M/B$ $k_q = 4.8\ E_M/B$

Where E_M = PMT modulus and B = Pile diameter

Racinais [26] notes that classical finite element input parameters are often very conservative for modelling CMCs. He has therefore made a study on calibrating soil parameters to Frank and Zhao [25] curves for numerical modelling of rigid inclusions using Plaxis software., and observed that increasing the cohesion and internal friction angle of the surrounding soil increased the ordinate of the curve's asymptote. Also, increasing the modulus of elasticity increased the slope of the elastic portion of the curve. Racinais was able to closely match Frank and Zhao curves by using soil parameters that necessarily do not have a physical interpretation. Initially, the value of skin fiction stress in the upper layers and 1/9 of base stress in the anchoring layer were assigned for cohesion, and null for the internal friction angle of the soils. Then the elastic modulus was trialled at various values, and it was observed that the closest match was achieved if the elasticity modulus was taken as $1.5E_M/\alpha$, where α is the PMT rheological factor.

2.6. CMC Inclusion Case Histories

Depth of CMC installation is practically limited by the equipment that are available. Whilst most rigs are capable of drilling to maximum depths ranging from approximately 20 to 28 m, CMCs have been installed to depths exceeding 30 m in Australia and the United States.

2.6.1. Previous World Record

CMCs have been installed to support five 12.8 m high steel oil tanks of an oil terminal that is located on the banks of the Mississippi River in New Orleans. Buschmeier et al. [27] have reported the installation depth to be 34 m, which to the knowledge of the authors makes these CMCs the world record for depth installation at the time of the project.

The diameters of three tanks are 39.6 m and two tanks are 45.7 m. The maximum pressure that the tanks exert on the ground is 130 kPa, and elevating the ground level to tank level has imposed an additional 16 kPa of pressure.

The superficial fill layer that is approximately 0.15 to 1.2 m thick is underlain by soft to medium stiff silty clays with some traces of organic matter and localised sand pockets, which extend down to depths of 4 to 6 m. This layer is followed by very soft clay with silt and sand that reach depths of 20 to 24 m. A thin sand layer was also identified at approximately 21 m depth. Medium stiff to stiff clay with fine sand pockets and shell fragments were observed to depths of up to 32 m followed by stiff to very stiff silty to sandy clays over a very dense layer of silty sands at depth of about 34 m. Groundwater level depth was less than 1 m below ground level.

Project specification stipulated that the tanks' maximum and central settlements be limited to respectively 200 and 100 mm and additionally 50 % of settlements allowed by American Petroleum Institute [28] three years after hydro-testing.

CMC were installed with a higher replacement ratio down to the depth of about 21 m where a sand layer with reduced compressibility was identified, and with a lower displacement ratio down to the maximum treatment depth at about 34 m.

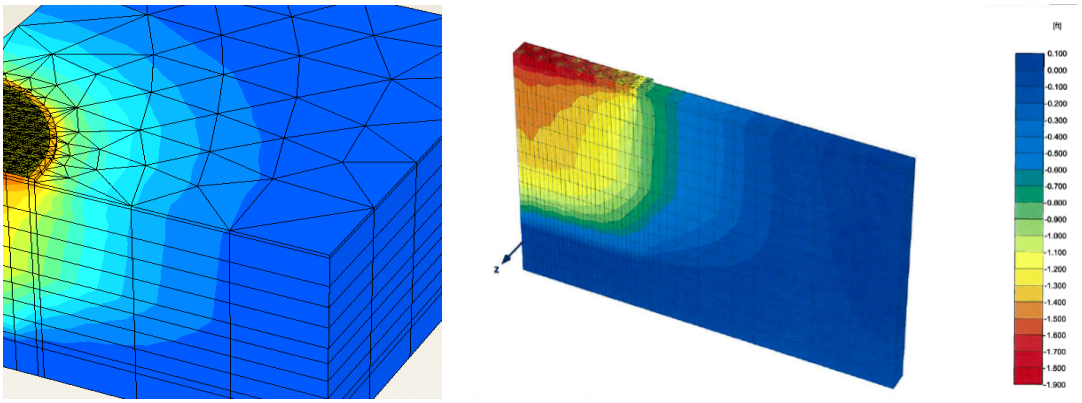

Fig. 22. Three-dimensional modelling of a quarter of a tank and a thin slice of the tank (Buschmeier et al [27])

Due to the variations in the soil profile it was necessary to design each tank individually. As shown in Figure 22, analyses included three-dimensional modelling of a quarter of a tank, three-dimensional modelling of a thin slice of the tank and manual calculations of rafts on floating piles.

CMC diameters for columns installed to approximately 21 m and 34 m were respectively 318 and 470 mm. Installation depth was variable for each tank due to variations in the site's soil profile.

2.6.2. Current World Record

Hamidi et al. [29] have reported the installation of 42 m long CMCs that to the knowledge of the authors are the world's deepest CMCs. This project is also located near New Orleans, and includes 4 oil tanks a water tank, two shop and maintenance buildings and ancillary structures. The diameter and height of the oil tanks are respectively 43.3 m and 11 m, and each tank will be filled with a product that will apply a design pressure of 120 kPa to the bottom of the tank.

Prior to construction, the site was relatively level and approximately at elevation ±0 m RL (reduced level). Initially, the uppermost 0.3 m of the ground was treated and modified to cement-stabilised clay. The site was then elevated with sand to +1.2 m RL. The tanks were built on 0.3 m thick pads.

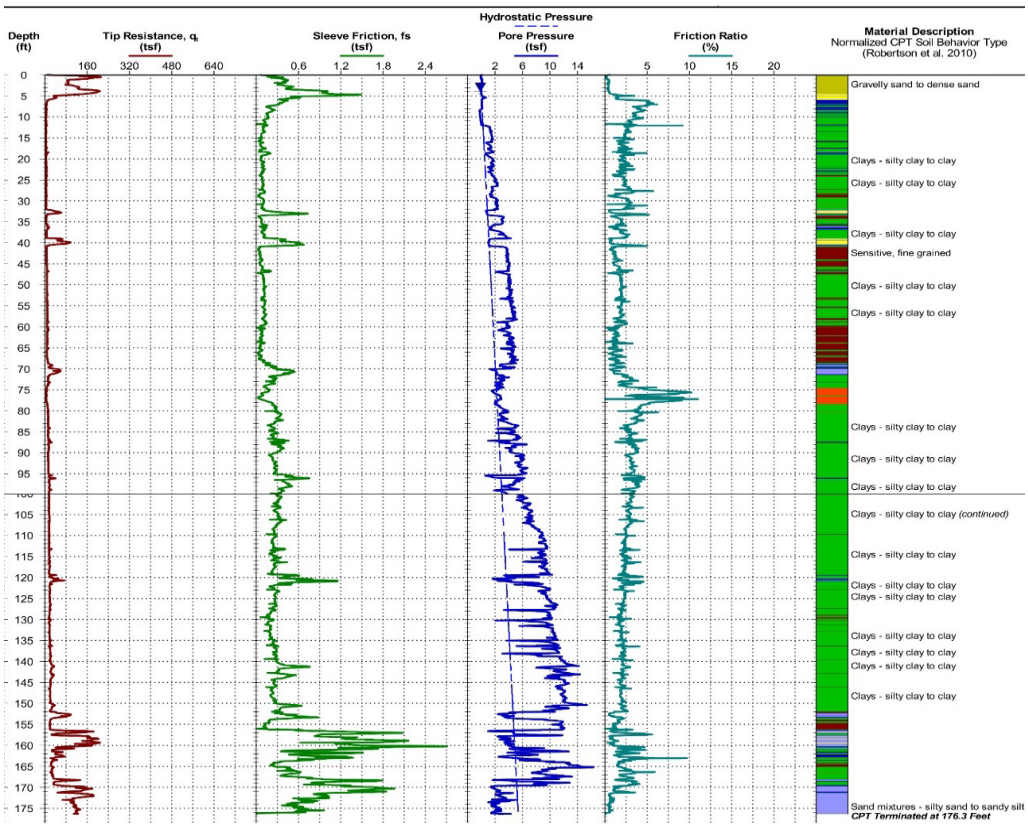

Fig. 23. CPT and soil profile of one of the tanks (note: units in empirical system)

The upper 1.5 to 3 m thick layer of ground consisted of a crust of desiccated over consolidated clay with an over consolidation ratio (*OCR*) of 4. Below this layer was a very soft clay layer that extended to depths of approximately 33.5 m. The *OCR* for this layer was assumed to decrease with depth from 3 in the upper part to 1.2 in the lower layers. A sand layer was present at depths of approximately 33 m to 36 m in some areas, but in other areas this layer was replaced by a stiff to medium stiff layer of clay roughly up to depths of 51 to 57 m. This lower clay was understood to have an OCR of 1.1. Cone Penetration Test (CPT) profiles at the location of the four tanks showed that the cone resistance was almost consistently very low and negligible in the soft clay. The CPT and soil profile of one of the tanks in shown in Figure 23.

Initial calculations indicated that the tanks were susceptible of undergoing settlements in the magnitude of 1.5 m to 1.8 m without implementation of an improved foundation system.

Since expected settlements exceeded the tank's design criteria that limited long term settlements under the tanks to 300 mm and differential settlements of values specified by American Petroleum Institute [28], specific geotechnical measures had to be implemented. The ground improvement contractor who was awarded the project proposed that three oil tanks be supported at the edge by a concrete slab and a geotextile-reinforced gravel ring wall while the fourth tank was designed to be supported by a load transfer platform and a geotextile-reinforced gravel ring wall. All structures were to be supported by CMCs installed in square grids that typically had 1.7 to 2.5 m spacing. Column diameters were 396 mm.

The design included an iterative approach and finite element analyses using a combination of three different modelling techniques; i.e. axi-symmetrical modelling, three-dimensional strip modelling, and three-dimensional global modelling. The calculation process was iterative as parameters needed to be adjusted in such a way that the various types of models yielded similar re-

sults. This approach led to approximately 280 mm of long term settlement under the centre of the tank, of which, 75 % occurred rather uniformly below the toes of the CMCs.

More than 2,600 CMCs were installed under the structures to an average depth of 36.5 m during a period of approximately 4 months.

Conclusion

Deep rigid inclusions have complicated the classical definitions of shallow and deep foundation systems. CMCs are a type of cementitious rigid inclusion that resemble piles, but their design concept is very different. They have many advantages, including independence of column strength from in-situ soil parameters, non-reliance of column lateral stability on in-situ soil parameters, significant reduction of the magnitude of settlements, vibration-less installation process, negligible amounts of spoil, and high production rates.

This technology utilises a load transfer platform to distribute the loads between the columns and the in-situ ground. Column loads can be determined by numerous methods. IREX proposes the analyses of ground behaviour and load distribution for grounds improved with columnar inclusions in a variety of cases.

Numerical methods are commonly used for the analysis of CMCs, but a deep insight is required for modelling and assigning input parameters in these methods. Research suggests that classical input parameters may over estimate settlements, and more accurate results may be possible if input parameters are calibrated. Racinais [26] has proposed a calibration method that is based on the pressuremeter test and matching the curves of Frank and Zhao [25].

CMCs have been successfully used for improvement of ground to depths of 42 m for highly strategic structures such as oil tanks.

References

1. Terzaghi K., Peck R.B., Mesri G. Soil mechanics in engineering practice. 3rd ed. New York, John Wiley and Sons, 1996, 512 p.

2. Bowles J.E. Foundation analysis and design. 5th ed. New York, McGraw Hill, 1996, 1175 p.

3. Das B.M. Shallow foundations bearing capacity and settlement. 2nd ed. Boca Raton, FL, USA, Taylor & Francis Group, 2009.

4. Prandtl L. Uber die härte plastischer Körper Nachrichten von der Königlichen Gesellschaft der Wissenschaften, Gottingen, *Math.-Phys. Klasse*, 1920, pp. 74–85.

5. Terzaghi K. Theoretical soil mechanics. New York, John Wiley & Sons, 1943, 510 p.

6. Meyerhof G.G. The ultimate bearing capacity of foundations. *Geotechnique,* 1951, vol. 2, iss. 4, pp. 301–333.

7. Hansen J.B. A revised and extended formula for bearing capacity. *Danish Geotechnical Institute Bulletin,* 1970, iss. 28 (successor to Bulletin No 11), p. 21.

8. Tomlinson M.J. Some effects of pile driving on skin friction. *Conference on Behaviour of Piles*, London, 1971, pp. 107–114.

9. Vijayvergiya V.N., Focht J.A. A new way to predict capacity of piles in clay. *4th Offshore Technology Conference*, Houston, 1972, paper 1718.

10. Burland J.B. Shaft friction piles in clay – a simple fundamental approach. *Ground Engineering,* 1973, vol. 6, iss. 3, pp. 30–42.

11. Chu J., Varaksin S., Klotz U., Mengé P. State of the art report: construction processes. *17th International Conference on Soil Mechanics & Geotechnical Engineering: TC17 meeting ground improvement*, Alexandria, Egypt, 7 October 2009, pp. 130.

12. Barksdale R.D., Bachus R.C. Design and construction of stone columns. Vol. 1, FHWA/RD-83/026. 1983, 194 p.

13. Navin M.P. Stability of embankments founded on soft soil improved with deep mixing method columns. PhD thesis, Virginia Polytechnic Institute and State University, 2005.

14. American Concrete Institute. Building Code Requirements for Structural Concrete (ACI 318-05) and Commentary (318R-05). Farmington Hills, MI, American Concrete Institute, 2005, 430 p.

15. Masse F., Pearlman S.L., Taube M.G. Controlled modulus columns for support of above ground storage tanks. *40th Ohio River Valley Soil Seminar (ORVSS),* Lexington, Kentucky, November 13, 2009.

16. Murayama S. Vibro-compozer method for clayey ground (in Japanese). *Mechanization of Construction Work,* 1962, iss. 150, pp. 10–15.

17. Aboshi H., Ichimoto E., Harada K. The Compozer: a method to improve characteristics of soft clays by inclusion of large diameter sand columns. *International Conference on Soil Reinforcement; Reinforced Earth and Other Techniques,* 2, Paris, 20–22 March, 1979, pp. 211–216.

18. Hamidi B., Nikraz H., Varaksin S. Arching in ground improvement.*Australian Geomechanics Journal*, 2009, iss. 44 (4 December), pp. 99–108.

19. Combarieu O. Amélioration des sols par inclusions rigides verticales. Application à l'édification de remblais sur sols médiocres. *Revue Française de Géotechnique,* 1988, vol. 44, pp. 57–79.

20. IREX. Recommandations pour la conception, le dimensionnement, l'exécution et le contrôle de l'amélioration des sols de fondation par inclusions rigides, ASIRI 384, Presses des Ponts. 2012.

21. European Standard. EN 1997-1: 2004, Eurocode 7: Geotechnical Design – Part 1: General Rules 171. 2004.

22. Okyay U.S. Etude expérimentale et numérique des transferts de charge dans un massif renforcé par inclusions rigides. Application à des cas de chargements statiques et dynamiques. *Civil and Environmental Engineering.* Lyon, Institut National des Sciences Appliquées de Lyon, 2010, 402 p.

23. European Standard. BS EN 1992-1-1, Eurocode 2: Design of Concrete Structures – Part 1-1: General – Common Rules for Building and Civil Engineering Structures. 2004.

24. Schweiger H.F. Results from numerical benchmark exercises in geotechnics. *5th European Conference Numerical Methods in Geotechnical Engineering (NUMGE 2002),* Paris, 4-6 September 2002, pp. 305–314.

25. Frank R., Zhao S.R. Estimation par les parametres pressiometriques de 1'enfoncementt sous charge axiale de pieux fores dans des sols fins. *Bulletin Laison Laboratoire Central des Ponts et Chaussees,* 1982, iss. 119, pp. 17–24.

26. Racinais J. Calibration of rigid inclusion parameters based on pressuremeter test results. *16th European Conference on Soil Mechanics and Geotechnical Engineering (XVI ESCMGE),* Edinburgh, 13–17 September 2015, Presentation.

27. Buschmeier B., Masse F., Swift S., Walker M. Full scale instrumented load test for support of oil tanks on deep soft clay deposits in Louisiana using controlled modulus columns. *International Symposium on Ground Improvement (IS-GI) Brussels 2012,* vol. 3, Brussels, 31 May – 1 June, 2012, pp. 359–372.

28. American Petroleum Institute. API Standard 653: Tank Inspection, Repair, Alteration, and Reconstruction, 3rd ed. 2001, 112 p.

29. Hamidi B., Masse F., Racinais J., Varaksin S. The boundary between deep foundations and ground improvement. *Geotechnical Engineering,* 2016, vol. 169, GE2, pp. 201–213.